Atmos. Meas. Tech. Discuss., 4, 969–1000, 2011
www.atmos-meas-tech-discuss.net/4/969/2011/
doi:10.5194/amtd-4-969-2011

Atmospheric Measurement Techniques Discussions

Can one detect small-scale turbulence from standard meteorological radiosondes?

R. Wilson[1], **F. Dalaudier**[2], **and H. Luce**[3]

[1]UPMC Univ Paris 06, Univ. Versailles St-Quentin, CNRS/INSU, UMR 8190, LATMOS-IPSL, Paris, France
[2]Univ. Versailles St-Quentin, UPMC Univ. Paris 06, CNRS/INSU, UMR 8190, LATMOS-IPSL, Paris, France
[3]Univ. du Sud Toulon-Var, CNRS/INSU, UMR 6017, LSEET, La Garde Cedex, France

Received: 23 November 2010 – Accepted: 27 January 2011 – Published: 10 February 2011

Correspondence to: R. Wilson (richard.wilson@upmc.fr)

Published by Copernicus Publications on behalf of the European Geosciences Union.

Abstract

It has been recently proposed by Clayson and Kantha (2008) to evaluate the climatology of atmospheric turbulence in the free atmosphere by applying a Thorpe analysis on standard radiosoundings obtained with relatively low resolution (LR) in the vertical. Since then, several studies based on this idea have been published. However, the impact of instrumental noise on the detection of turbulent layers was completely ignored in these works. The present study aims to evaluate the feasibility of turbulence detection from radiosoundings. For this purpose, we analyzed data of two field campaigns during which high-resolution (HR) soundings (10–20 cm) were performed simultaneously with standard LR soundings. We here used the raw data of standard radiosondes, the vertical resolution ranging from 5 to 8 m.

A Thorpe analysis was performed on both LR and HR potential temperature profiles. A denoising procedure was first applied in order to reduce the probability of occurrence of artificial inversions, i.e. inversions due to instrumental noise only. We then compare the empirical probability of the sizes of the selected overturns from LR and HR profiles.

From HR profiles in the troposphere, the scales of the detected turbulent overturns range from 4 to ~1000 m. The shape of the distribution of the size of overturns is found to sharply decrease with increasing scales. From LR profiles, the smallest scale of detected overturns is ~32 m, a similar decrease in the shape of the size distribution being observed. These results suggest that turbulent events can indeed be detected from standard radiosondes measurements in the troposphere. However these events are rather rare as they belong to the tail of the size distribution of the turbulent overturns: they only represent the 7% largest events. Similar conclusions are obtained from radiosondes data collected in the lower stratosphere, but the fraction of the detectable events is even smaller than in the troposphere since they are the 4% largest events.

AMTD

4, 969–1000, 2011

1 Introduction

Thorpe (1977) proposed an elegant and simple-to-use method allowing to identify and to characterize turbulent patches from in situ measurements in oceans and lakes. The method is based on the comparison between an observed vertical profile of potential density and a reference profile corresponding to a minimum state of available potential energy. The reference profile is built by sorting in increasing order the observed potential density profile. It corresponds to an adiabatic re-arrangement of the observed fluid parcels. This method can be applied to atmospheric data as well by considering potential temperature instead of potential density. Since a vertical profile of potential temperature (potential density) in a stably stratified fluid is a monotonic function of altitude (depth), overturns display clear differences between the measured and sorted profiles. Such overturns are the signature of convective instabilities which in turn produce turbulent mixing.

The Thorpe method can a priori be applied to standard soundings data, either conductivity-temperature-density (CTD) in the ocean or lakes, (e.g. Thorpe, 1977; Galbraith and Kelley, 1996; Ferron et al., 1998; Alford and Pinkel, 2000) or pressure-temperature (PT) in the atmosphere (Luce et al., 2002; Gavrilov et al., 2005; Clayson and Kantha, 2008; Wilson et al., 2010). It has been recently proposed by Clayson and Kantha (2008) to apply Thorpe analyses to the huge data-base of meteorological radiosondes (RS), in order to infer the space-time variability of atmospheric turbulence in the free atmosphere. Since then, several such studies were published (Alappattu and Kunhikrishnan, 2010; Nath et al., 2010). Also, Balsley et al. (2010) proposed to use slow ascent radiosondes for observing turbulence in the atmosphere.

However, the issue of instrumental noise was not addressed at all in these aforementioned works. From our point of view, the issue of noise is a key point of the Thorpe method, that must be treated with great care. Oceanographers long-time know that instrumental noise can generate artificial inversions which are very difficult to distinguish from real ones (Thorpe, 1977; Galbraith and Kelley, 1996; Ferron et al., 1998; Gargett

AMTD
4, 969–1000, 2011

and Garner, 2008, e.g., among others). Surprisingly, although few exceptions exist (e.g. Gavrilov et al., 2005; Wilson et al., 2010), the issue of noise is generally ignored in most studies dealing with atmospheric turbulence owing to the fact that: "it is less of an issue in the free atmosphere, where the mean overall stratification is quite strong..." Clayson and Kantha (2008). From our point of view, as shown by Wilson et al. (2010), this affirmation does not hold, neither for standard meteorological measurements, nor for HR atmospheric measurements, because nearly neutral layers are very common.

Hereafter, according to the terminology used by Johnson and Garrett (2004), an *inversion* is defined as a localized decrease of potential temperature versus height, whatever its origin may be, either induced by turbulent motions or by noise. The term *overturn* will specifically refer to an inversion resulting from atmospheric motions (turbulence or convective overturns produced by Kelvin-Helmholtz instabilities or gravity waves). The selection of artificial inversions as turbulent overturns, may result in a dramatic overestimation of the frequency of occurrence of turbulent events, thus leading to overestimations of both the turbulent fraction of the atmosphere and the turbulence energy. The space-time inhomogeneity of turbulence can give rise to diffusion coefficient estimates ranging over several orders of magnitude Wilson (2004). It is therefore crucial to apply a quantitative procedure allowing to discriminate turbulent overturns from noise-induced inversions.

A quantitative method for selecting overturns in a potential temperature (or potential density) profile has been recently proposed by Wilson et al. (2010). The method is based on a hypothesis test on an order statistics, the data range within the detected inversions. The range of a sample is defined as the difference between the maximum and the minimum values in that sample. The detected inversions which cannot be distinguished from artificial inversions, that is inversions induced by instrumental noise, are not selected as overturns. The selection method will be described in more details later.

AMTD
4, 969–1000, 2011

The present paper addresses the following two questions:

1. Can we detect small scale turbulence from standard radiosondes in the troposphere and lower stratosphere?

2. If yes, what are the scales of the detectable events considering the vertical resolution and the noise level of radiosonde measurements?

In order to address these issues, we analyzed the datasets of two field campaigns during which high-resolution (HR) balloon soundings and standard RS were simultaneously performed: the SFT campaign (1998) and the MUTSI campaign (2000). (SFT stands for Structure Fine de Temperature) and MUTSI for MU radar, Temperature Sheets and Interferometry). Seven (forteen) RS were launched during the SFT and MUTSI campaigns respectively. One of the seven LR flights of the SFT campaign is not used in this study as the ascent speed was abnormally slow.

The paper is structured as follows. The datasets and data processing methods are described in Sect. 2. The analysis methods of the potential temperature profiles are presented in Sect. 3, a quantitative criterion for the selection of the turbulent overturns being described. In Sect. 4, we present the distribution in size of the selected overturns from both LR and HR profiles in the troposphere and in the lower stratosphere. Discussion and conclusions are given in the final section.

2 Dataset and processing of the raw data

2.1 The datasets

Standard atmospheric RS provide temperature, pressure and humidity measurements. With the aim of detecting small scale motions, we used the raw data of standard radiosondes during the SFT and MUTSI campaigns. The standard soundings were performed by Vaisala radiosondes RS80G (SFT) and RS90G (MUTSI) at an initial

AMTD
4, 969–1000, 2011

sampling frequency of 0.7 Hz. The vertical resolution is variable due to the fluctuations of the vertical ascent velocity of the balloon.

For each of the campaigns (SFT and MUTSI), three of the balloons carried both HR and LR sensors. The HR profiles were acquired with a sampling frequency of 25 Hz for the SFT flights and 50 Hz for the MUTSI flights. The reader can find more details about the HR measurements in Luce et al. (2002) and Gavrilov et al. (2005). The HR and LR sensors were on the same gondola, and the data were acquired simultaneously.

2.2 Construction of potential temperature profiles from raw data of radiosondes

For the RS80 and RS90 Vaisala radiosondes used in this study, the measured temperature and pressure are quantized with a resolution of 0.1 K and 10 Pa respectively. As previously mentionned, the measurements are irregularly sampled with altitude.

In order to perform a Thorpe analysis, it is necessary to dispose of data sampled with a regular vertical step, the reference profile being a vertical rearrangement of the observed profile. The measured profiles need to be resampled with a regular vertical interval δz. The first task is to estimate the altitude of the measurements. By assuming hydrostatic equilibrium, the i-th altitude difference, $\Delta z_i^{\mathrm{M}} = z_{i+1}^{\mathrm{M}} - z_i^{\mathrm{M}}$, inferred from the measured pressure and temperature at level i, P_i^{M} and T_i^{M} respectively, is given by

$$\Delta z_i^{\mathrm{M}} = -\frac{R\, T_i^{\mathrm{M}}}{g_i}\,\frac{\Delta P_i^{\mathrm{M}}}{P_i^{\mathrm{M}}} \tag{1}$$

R being the gas constant for air ($\mathrm{J\,kg^{-1}}$) and g_i the acceleration of gravity at level i. The superscript "M" stands for "measured". The i-th altitude level is simply

$$z_i^{\mathrm{M}} = z_0 + \sum_{k=0}^{i-1} \Delta z_k^{\mathrm{M}} \tag{2}$$

Due to quantization, the first differences of the measured pressure are not always negative (as it should be during the ascent of the balloon) especially for high altitude

AMTD
4, 969–1000, 2011

levels, i.e. above 20 km altitude. The top panel of Fig. 1 shows the first differences of pressure measurements (cyan curve). It is observed that quantization effects are increasingly important with increasing altitudes. As a consequence, the calculated raw altitude, z^{M}, from the measured pressure are not monotonically increasing during the ascent of the balloon: the altitude differences are quantized, the vertical steps growing with increasing altitudes (Fig. 1, lower panel), some differences being negative. Consequently, the raw altitudes z^{M} cannot be used for building the vertical profile.

A monotonic pressure is desirable for overcoming this difficulty. For that purpose, we estimate the pressure, P^{A}, which, if quantized, would give the measured pressure, P^{M}. The pressure P^{A} is evaluated through a least square cubic spline approximation (superscript "A" stands for "approximation"). The black curve of the upper panel of Fig. 1 shows the first differences ΔP^{A} which is cleanly negative for all levels. The altitude of measurements z^{A} is estimated from Eq. (1) but by using P^{A} instead of P^{M}. On the lower panel of Fig. 1, the black curve shows the first differences of altitudes Δz^{A} estimated from P^{A} and T^{M}. The vertical steps are found to range from 5 to 9 m, owing to the variations in the balloon ascent velocity.

For this particular flight (MUTSI-LR10) an average height interval of 7 m is found. The measured temperature T^{M} and approximated pressure P^{A} are interpolated with a regular vertical step of 7 m. One can use here, either a linear interpolation or a cubic spline interpolation, the differences between these two methods being found to be unimportant. The interpolated temperature and pressure, T^{I} and P^{I}, respectively are the data analyzed in this work. Figure 2 (left panel) shows the temperature profile of flight LR10 of the MUTSI campaign. The curves show the temperature plus and minus two standard deviations of noise (only visible on the magnifying panel). The method by which the instrumental noise is estimated will be described in Sect. 2.3 of this section.

The pressure, temperature and altitude are not independent quantities as they are related through the hydrostatic equilibrium relationship (Eq. 1). The knowledge of two of the three quantities completely determines the third one. For instance, the knowledge

AMTD
4, 969–1000, 2011

of T^{I} regularly sampled with step δz allows to calculate the vertical profile of pressure for the same altitudes. The calculated pressure from T_i^{I} is almost indistinguishable from the interpolated pressure P_i^{I} although T and P are independantly measured: they differs by less than 0.02 Pa in the average, giving thus strong confidence in the data processing method.

After re-sampling at a constant vertical step, the vertical resolution of LR temperature and pressure profiles is ∼6–7 m, depending on the flight. The vertical resolution of the resampled HR profiles is ∼20 cm (10 cm) for the SFT and MUTSI datasets, respectively.

The potential temperature θ is inferred from the resampled temperature and pressure, T_i^{I} and P_i^{I}, by using the relation for ideal diatomic gas:

$$\theta_i = T_i^{\mathrm{I}} \left(\frac{1000}{P_i^{\mathrm{I}}} \right)^{2/7} \tag{3}$$

where T is the temperature (K), and P the pressure (hPa). The right panel of Fig. (2) shows the potential temperature plus and minus two standard deviations of noise. Several thick nearly neutral layers can be seen in the troposphere, around 4 km altitude and above 10 km altitude as well as in the stratosphere, below 20 km altitude.

2.3 Estimation of instrumental noise

A key point of the selection method (presented in the next section) is to estimate the noise on potential temperature resulting from instrumental noise on T and P. The noise standard deviations for the LR and HR data are experimentally estimated from both the temperature and pressure resampled profiles. After comparing several methods, some of them based on spectral or on wavelet analyses, we finally retained a simple-to-use method based on the estimate of the variance of the first differences of the data (T or $\ln P$). One important outcome of these tests is that the instrumental noise on temperature and pressure depends on altitude for both the LR and HR profiles.

AMTD
4, 969–1000, 2011

Therefore, we must estimate a vertical profile of the instrumental noise level. The method for estimating the noise level is the following:

1. Spliting the entire profile in short segments of about 200 m length (32 or 2000 points according to the vertical resolution).
2. Removing a linear trend for each sequence.
3. Calculating the variance of data first differences. This variance is an estimate of twice the noise variance.
4. Smoothing the resulting noise profile.

Figure 3 shows the estimated level of instrumental noise for the temperature and pressure measurements for flight MUTSI-LR10. The stairs step curve shows the noise estimates for each data segment, the smoothed curve showing the noise level profile after smooting (here a least square spline approximation). For the pressure measurements, the noise is estimated from the logarithm of the measurements in order to apply a linear dedrending (step 2).

For the twenty LR flights of the SFT and MUTSI campaigns, the averaged noise standard deviation of the resampled temperature profile is found to be 27 mK. For the six HR flights, the noise standard deviation of temperature data is found to be 4 mK in the average. The noise level of the LR temperature measurements is observed to slightly decrease with altitude (Fig. 3). The noise standard deviation of the resampled pressure profile is found to be negligible: 3×10^{-2} Pa in the average. Consequently, the noise on the potential temperature depends primarily on the instrumental noise of temperature measurements. From Eq. (3), the standard deviation of noise of potential temperature, σ_θ is estimated by

$$\sigma_\theta = \theta \sqrt{\left(\frac{\sigma_T}{T}\right)^2 + \left(\frac{2}{7}\frac{\sigma_P}{P}\right)^2} \approx \theta \frac{\sigma_T}{T} = \left(\frac{1000}{P}\right)^{2/7} \sigma_T \quad (4)$$

AMTD
4, 969–1000, 2011

where σ_T (σ_P) are the noise standard deviation of temperature and pressure respectively. The noise level of potential temperature grows with altitude, due to the pressure term of Eq. (4): it increases from ∼35 to ∼70 mK (2.6 to 3.5 mK) for LR (respectively HR) profiles for heights ranging from the ground level up to 27 km.

3 Analyse method of the potential temperature profiles

3.1 Selection method of the overturns

In order to evaluate the filtering effects due to both the vertical resolution and the level of instrumental noise, we analyzed the profiles by using an identical selection criterion. For discriminating the turbulent overturns from artificial inversions, i.e. inversions induced by noise, we used a hypothesis test on the data range statistics. The method is described in details in Wilson et al. (2010). Here, we shortly describe the three key steps of the method.

1. *Determination of the optimal vertical resolution.* We first estimate the vertical resolution that should be used by taking account for the mean stratification and the level of the instrumental noise. Such a resolution can be inferred from the bulk trend-to-noise ratio (tnr), $\overline{\zeta}$ of the profile. The bulk tnr, $\overline{\zeta}$, is a measure of the average of first differences of the data (potential temperature) $\overline{\tau}$, scaled by the noise σ_N:

$$\overline{\zeta} = \frac{\overline{\tau}}{\sigma_N} \tag{5}$$

with

$$\overline{\tau} = \overline{\theta_{i+1} - \theta_i} = \frac{1}{n-1}(\theta_n - \theta_1) \tag{6}$$

AMTD
4, 969–1000, 2011

where θ_i is the potential temperature measured at altitude z_i ($1 \leq i \leq n$). The average of first differences τ depends on both the stratification and the vertical resolution since

$$\overline{\tau} = \overline{\frac{\partial\theta}{\partial z}}\delta z \tag{7}$$

where z is the vertical coordinate and δz the (constant) vertical step. The bulk tnr gives an indication on the minimum size for the overturns to be detectable (Wilson et al., 2010). The smaller $\overline{\zeta}$ is, the larger the data sample must be in order to be distinguishable from a pure noise sample. If $\overline{\zeta}$ is too small (smaller than one typically), a preliminary denoising procedure is required. The denoising is based on both a filtering and an undersampling of the data. It aims at increasing the tnr while preserving the independence of the noise for each data bins. The tnr of the degraded data increases by a factor $m^{3/2}$ where m is the undersampling factor (i.e. the number of bins of the running filter).

2. *Detection of the inversions.* The potential temperature profile (denoised if needed) is sorted. The Thorpe displacements profile can then be estimated. The (artificial and real) inversions are detected from the cumulative sum of the Thorpe displacements since the sum of Thorpe displacements is null within an inversion.

3. *Selection of the overturns.* An inversion is identified as an overturn if the range of the data belonging to the inversion exceeds a large prescribed percentile of the range of a noise sample of same size and standard deviation equal to that of the instrumental noise. For practical purpose, we tabulated the moments of the range, as well as various percentiles, for normally distributed variables as a function of the sample size (ftp.aero.jussieu.fr/pub/os/WN.txt).

The vertical profile of tnr ζ_{LR} for the MUTSI-LR10 flight is shown in Fig. 4a. The bulk tnr $\overline{\zeta}_{LR}$ is ~0.9 (dashed line), the local values showing minima smaller than 10^{-1} around

AMTD
4, 969–1000, 2011

11 km altitude. For such a bulk tnr, one cannot expect to identify overturns smaller than $n \sim 60$ bins, that is thinner than ∼420 m (see Fig. 5 of Wilson et al., 2010). In order to improve the dedection threshold, a denoising procedure is required. For the region with tnr of 0.1, an undersampling $m = 2$ allows to reach a local tnr of $2\sqrt{2} \times 10^{-1} \approx 0.3$, allowing to detect overturns of 20 bins, i.e. $20 \times 14 = 280$ m.

3.2 Overturns selection

The average tnr being less than 1 for both LR and HR profiles in the troposphere, a denoising procedure is applied on the two datasets. The undersampling factor is 2 for the LR data, and is 5 (11) for the HR data of the SFT and MUTSI flights respectively. The bulk tnr reaches 2–3 for both datasets. Consequently, the vertical resolution is ∼12 m for the LR profiles, and is 1 m (SFT) or 1.1 m (MUTSI) for the HR profiles.

Owing to the stronger stability in the stratosphere the tnr of both LR and HR data is substantially larger than in the troposphere. Consequently, the undersampling factor required to reach a tnr of ∼2–3 is smaller than in the troposphere, allowing to get better vertical resolutions. The vertical resolution of the LR data is ∼6 m (no undersampling required) whereas the vertical resolution of the HR data is ∼0.5 m.

In order to evaluate the impact of the selection method (including the denoising procedure) we compare the results of Thorpe analyses without and with a selection procedure. Figure 5 shows the histograms of the number of occurrences of inversions (blue-filled) and overturns (red-transparent) as a function of their sizes for all the LR profiles. The distribution of the detected inversions (blue-filled histogram) results from the original potential temperature profiles (vertical resolution ∼6 m), without applying any denoising and selection procedure. The distribution of the selected overturns for the same LR data (red-transparent histogram) results from the denoised (undersampled and filtered) profiles (vertical resolution ∼12 m). The selection procedure allows to retain as overturns 11% of the detected inversions only. Consequently, due to both the noise level of standard RS data and the average stratification of the troposphere, a very large fraction of detected inversion can be due to instrumental noise only. It is

AMTD
4, 969–1000, 2011

therefore indispensable to apply a selection procedure in order to identify real turbulent patches, at least in the troposphere.

4 Size distribution of the detected overturns

We analyzed the LR and HR profiles by using the same selection method for detecting the turbulent patches. As mentioned in the previous section, the bulk tnr $\overline{\zeta}$ of all profiles ranges from 2 to 3 after applying the denoising procedure. We present in this section the empirical probability, that is the relative frequency, of the sizes of the selected overturns from both datasets, LR and HR, in the troposphere and in the stratosphere.

4.1 Results for tropospheric data

Figure 6 shows the number of occurrences of Thorpe displacements (in absolute value) as a function of their sizes for the six HR profiles. The two histogram results from all displacements found within the selected overturns in the troposphere, the green-filled histogram corresponding to HR profiles whereas the red-transparent histogram results from the LR profiles. Due to the large dynamic of the observed values, the histograms are shown in a log-log scale. The widths of the intervals (abscissa) being constant on a log scale, they increase as a power law. We simply used a dyadic scale, the maximum value of each interval being equal to twice the minimum value (i.e. 1–2 m, 2–4 m, etc.). The number of occurrences are not directly comparable because the vertical step of LR profile is here about 12 times larger than that of HR profiles (12 m vs. 1 m). The considered displacements range from 1 m to ∼500 m and from 12 to ∼1000 m for the HR and LR profiles, respectively. As expected, the smallest displacements corresponds to the vertical resolution, ∼1 m (within the 1–2 m interval) for HR data and ∼10 m (within the 8–16 m interval) for LR data.

On an other hand, few displacements observed from LR profiles (about 20 occurrences) are larger than the largest displacement obtained from HR profiles. Such larger

AMTD
4, 969–1000, 2011

displacements in the LR profile are likely the consequence of the poorer vertical resolution. Indeed, the LR profiles does not always allow to identify distinct turbulent patches within weakly stratified regions. Such regions may appear as a single overturn in the LR profile, whereas the HR profiles reveals several distinct overturns. Several examples of such merged patches can be seen in the paper of Wilson et al. (2010). The largest LR displacements likely belongs to these merged patches. This last result can have impact on the determination of the Thorpe lengths, and on the inferred turbulence parameters, from LR profiles in weakly stable regions.

The two histograms of Fig. (6) are proportional to the empirical probability of Thorpe displacements. They reveal a tendency for the probability density function (pdf) of displacements to decrease with increasing scale. The pdf from LR measurements appears similar in shape but shifted by about 10 m toward larger scales.

Next, we consider the size of the selected overturns, i.e. their vertical extent. The empirical probability of the overturns sizes for both LR and HR profiles are shown in the left panel of Fig. 7, the right panel showing the occurrence number of overturns according to their size. The empirical probabilities are of course proportional to the number of occurences. However, the plot of occurrence number (right panel) allows a direct comparison of the numbers of events independently detected from HR and LR data during the six HR/LR flights. It is observed that the smallest overturns from HR data fall within the 4–8 m interval whereas the smallest overturns from LR data are within the 32–64 m interval. It should be noticed the the inner scale of turbulence, which ranges from ∼0.1 to 10 cm in the free troposphere and lower stratosphere (Eaton and Nastrom, 1998), is much smaller than the smallest scale observable from the HR profiles. Consequently, the decrease in number of occurrences for smallest size in HR is a cutoff effect similar to the one observed at much larger sizes for the LR data. The relatives frequencies and the cumulative distributions of the overturns sizes are detailed in Table 1. It is found that 93% of the overturns identified from the HR profiles are smaller than 32 m, i.e. smaller than the smallest overturns detected from LR profiles. These observations demonstrate that, from LR profiles in the troposphere, it is only possible

AMTD
4, 969–1000, 2011

to identify those overturns belonging to the tail of the size distribution. The selected overturns from LR profiles represent ∼7% of the overturns found from HR profiles. On the other hand, the number of selected overturns from HR and LR profiles compares quite well, except for the smallest overturns in the LR profiles. (the number of overturns in the HR profiles is about 3 times the number of overturns from the LR profiles for the 32–64 m interval). Although a large number of small overturns are missed, this last result suggests that the largest overturns are correctly identified from LR radiosonde profiles.

Figure 8 shows the empirical probability of the sizes of turbulent overturns for all the flights, that is the six HR and twenty LR profiles of the MUTSI and SFT campaigns, in the troposphere. Again, the smallest overturns of the LR profiles are in the 32–64 m interval. Also, one observes that the shape of the two probability distributions compare quite well, as both distributions decrease with a comparable rate. This observation suggests that the tail of the distribution in size of the overturns is correctly sampled from LR profiles (except maybe for the extreme values, i.e. for the first and last intervals).

4.2 Results for stratospheric data

The same selection method was applied to the stratospheric profiles. Figure 9 shows the distribution of the number of occurrences of Thorpe displacements for the selected overturns (HR and LR) in the stratosphere for the six HR profiles. Here, the Thorpe displacements range from 0.5 to ∼50 m for the HR profiles, and from 6 to ∼200 m for the LR profiles. Again, the few larger displacements from LR data (less than 20 occurrences) are likely due to the much lower resolution of LR profiles, leading to a poor definition of the turbulent patches within weakly stable regions.

The left panel of Fig. 10 shows the empirical probability of the sizes of turbulent overturns in the stratosphere for the six HR profiles. From HR profiles, the size of overturns now ranges from 2 to ∼100 m. The relative frequencies of overturns size are observed to sharply decrease with increasing sizes. From LR profiles, the overturns size ranges from ∼25 m (16–32 m) to ∼200 m (128–256 m). Table 2 gives the

AMTD
4, 969–1000, 2011

cumulative frequencies of the overturns size. It is observed that 96% of the selected overturns from HR profiles have a size smaller than 16 m (Table 2). The right panel of Fig. 10 shows the number of occurrences of the overturns size for these six HR profiles. A striking feature is the small number of selected overturns from the six LR profiles: 85 events, i.e. about foorteen per profile for all the sounded stratosphere (roughly from 10 to 25 km). As in the troposphere, the number of occurrences of selected overturns according to their sizes is very similar for LR and HR profiles (except for the smallest class, i.e. 16–32 m, for the LR profiles). One can again conclude that, within the stratosphere, the overturns which size is larger than ∼25 m are correctly sampled from LR profiles. But such turbulent patches are rather rare in the stratosphere since they only represent about 4% of all the turbulent events detected from HR profiles.

Figure 11 shows the empirical probability of the overturns size in the stratosphere for all the (six HR and twenty LR) profiles. The sizes of overturns from LR profiles now range from ∼25 to 512–1024 m. Both distributions are sharply decreasing with increasing scales. The shape of the two distributions are very similar, giving confidence in the detection of the larger turbulent events from LR profiles. Again, the scales for which LR overturns are detected and selected represent only 4% of the HR overturns since the selection procedude do not allow to retain overturns smaller than 16 m from LR data.

5 Conclusions

We have analyzed a dataset of balloon soundings obtained during two field campaigns. The dataset includes six HR profiles (10–20 cm) and twenty LR profiles (6–7 m). The HR and LR profiles were obtained simultaneously, the sensors being on the same gondola. The LR profiles results from raw profiles collected by radiosondes vertically resampled at a regular step (6 or 7 m).

After applying a denoising treatment, we performed a Thorpe analysis. We applied a selection method allowing to reject artificial inversions, or more precisely inversions

AMTD
4, 969–1000, 2011

that cannot be distinguished from noise induced inversions. We can only retained 11.4% (25%) of the detected inversions as real overturns from LR (respectively HR) profiles in the troposphere. In the stratosphere, the situation is worse as the noise on potential temperature increases whereas the scale of the turbulent events diminishes. Only 7.9% (20.8%) of the detected inversions are selected as overturns from the LR (respectively HR) profiles. Consequently, for detecting atmospheric turbulence by a Thorpe analysis, the instrumental noise is a key issue which must be treated with great care in the troposphere as well as in the stratosphere.

An important conclusion of this work is that, despite the above mentioned limitations and difficulties, it is possible to detect overturns resulting from atmospheric turbulence from the raw data of standard radiosondes sampled at a rate of 0.7 Hz. However, we showed that only the deepest turbulent patches corresponding to the tail of the size distribution, can effectively be detected from RS, in the troposphere as well as in the stratosphere. From our data set, the detectable overturns from RS in the troposphere corresponds to the 7% largest events that are observed from HR profiles. In the stratosphere, the detected patches from RS correspond to about the 4% largest events.

This last conclusion opens interesting perspectives about the means of observing turbulence in the free atmosphere. Indeed, provided raw data of radiosondes are available, and by applying a rigorous treatment for the instrumental noise, the huge data base of standard radiosoundings can be used in order to characterize the climatology of atmospheric turbulence, at least for the most energetics events.

AMTD
4, 969–1000, 2011

Acknowledgements. The authors wish to acknowledge CNES (Centre National d'Études Spatiales) for operating the balloons in Japan and the Research Institute for Sustainable Humanosphere (RISH) for their contribution in the MUTSI campaign.

The publication of this article is financed by CNRS-INSU.

References

Alappattu, D. P. and Kunhikrishnan, P. K.: First observations of turbulence parameters in the troposphere over the Bay of Bengal and the Arabian Sea using radiosonde, J. Geophys. Res., 115, D06105, doi:10.1029/2009JD012916, 2010. 971

Alford, M. H. and Pinkel, R.: Observation of overturning in the thermocline: The context of ocean mixing, J. Phys. Oceanogr., 30, 805–832, 2000. 971

Balsley, B., Kantha, L., and Colgan, W.: On the use of Slow Ascent Meter-Scale (SAMS) Radiosondes for observing overturning events in the free atmosphere, J. Atmos. Ocean. Tech., 27, 766–775, 2010. 971

Clayson, C. A. and Kantha, L.: On Turbulence and Mixing in the Free Atmosphere Inferred from High-Resolution Soundings, J. Atmos. Ocean. Tech., 25, 833–852, 2008. 970, 971, 972

Eaton, F. D. and Nastrom, G. D.: Preliminary estimates of the vertical profiles of inner and outer scales from White Sands Missile Range, New Mexico, VHF radar observation, Radio Sci., 33, 895–903, 1998. 982

Ferron, B., Mercier, H., Speer, K., Gargett, A., and Polzin, K.: Mixing in the Romanche fracture zone, J. Phys. Oceanogr., 28, 1929–1945, 1998. 971

Galbraith, P. S. and Kelley, D. E.: Identifying overturns in CDT profiles, J. Atmos. Ocean. Tech., 13, 688–702, 1996. 971

AMTD

4, 969–1000, 2011

Gargett, A. E. and Garner, T.: Determining Thorpe Scales from Ship-Lowered CTD density profiles, J. Atmos. Ocean. Tech., 25, 1657–1670, 2008. 971

Gavrilov, N. M., Luce, H., Crochet, M., Dalaudier, F., and Fukao, S.: Turbulence parameter estimations from high-resolution balloon temperature measurements of the MUTSI-2000 campaign, Ann. Geophys., 23, 2401–2413, doi:10.5194/angeo-23-2401-2005, 2005. 971, 972, 974

Johnson, H. L. and Garrett, C.: Effect of noise on Thorpe Scales and run lengths, J. Phys. Oceanogr., 34, 2359–2372, 2004. 972

Luce, H., Fukao, S., Dalaudier, F., and Crochet, M.: Strong mixing events observed near the tropopause with the MU radar and hight-resolution Balloon techniques, J. Atmos. Sci., 59, 2885–2896, 2002. 971, 974

Nath, D., Venkat Ratman, M., Patra, A. K., Krishna Murthy, B. V., and Bhaskar Rao, S. V.: Turbulence characteristics over tropical station Gadanki (13.5° N, 79.2° E) estimated using high-resolution GPS radiosonde data, J. Geophys. Res., 115, D07102, doi:10.1029/2009JD012347, 2010. 971

Thorpe, S. A.: Turbulence and mixing in a Scottish Lock, Philos. T. Roy. Soc. Lond. A, 286, 125–181, 1977. 971

Wilson, R.: Turbulent diffusivity in the free atmosphere inferred from MST radar measurements: a review, Ann. Geophys., 22, 3869–3887, doi:10.5194/angeo-22-3869-2004, 2004. 972

Wilson, R., Luce, H., Dalaudier, F., and Lefrère, J.: Turbulent Patch Identification in Potential Density/Temperature Profiles, J. Atmos. Ocean. Tech., 26, 977–993, 2010. 971, 972, 978, 979, 980, 982

AMTD
4, 969–1000, 2011

Table 1. Number of occurrences and cumulative frequencies (brackets) of the size of selected overturns in the troposphere, for the MUTSI and SFT campaigns (6 HR and 20 LR profiles).

Sizes (m)	2–4	4–8	8–16	16–32	32–64	64–128	128–256	256–512	512–1024
HR	245 (0.09)	1307 (0.58)	668 (0.82)	280 (0.93)	131 (0.98)	38 (0.992)	14 (0.997)	5 (0.999)	3 (1)
LR (HR flights)	0 (0)	0 (0)	0 (0)	0 (0)	43 (0.36)	48 (0.76)	19 (0.92)	4 (0.95)	4 (0.98)
LR (all flights)	0 (0)	0 (0)	0 (0)	0 (0)	153 (0.35)	166 (0.76)	78 (0.92)	22 (0.97)	12 (0.99)

AMTD
4, 969–1000, 2011

Table 2. Number of occurrences and cumulative frequencies (brackets) of the size of selected overturns in the stratosphere, for the MUTSI and SFT campaigns (6 HR and 20 LR profiles).

Sizes (m)	2–4	4–8	8–16	16–32	32–64	64–128	128–256	256–512	512–1024
HR	1960 (0.46)	1517 (0.81)	583 (0.95)	188 (0.990)	36 (0.998)	8 (1)	0 (1)	0 (1)	0 (1)
LR (HR flights)	0 (0)	0 (0)	0 (0)	33 (0.39)	39 (0.85)	9 (0.95)	4 (1)	0 (1)	0 (1)
LR (all flights)	0 (0)	0 (0)	0 (0)	419 (0.68)	115 (0.87)	50 (0.95)	16 (0.98)	11 (0.998)	1 (1)

AMTD
4, 969–1000, 2011

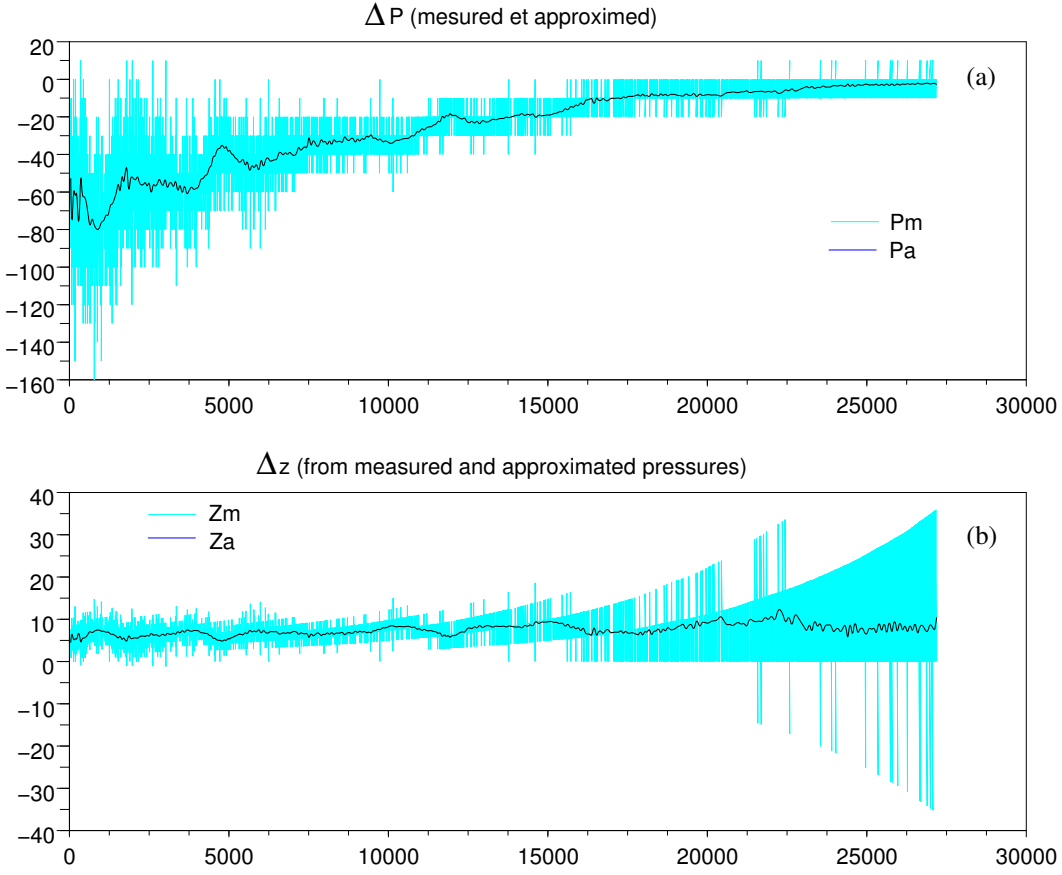

Fig. 1. **(a)** First differences of measured pressure ΔP (cyan) and approximated pressures (black) for thr MUTSI-LR10 flight. **(b)** The first difference of altitudes Δz inferred from raw measurements (cyan) and by using the approximated pressures (black).

AMTD
4, 969–1000, 2011

Small-scale turbulence from standard radiosondes

R. Wilson et al.

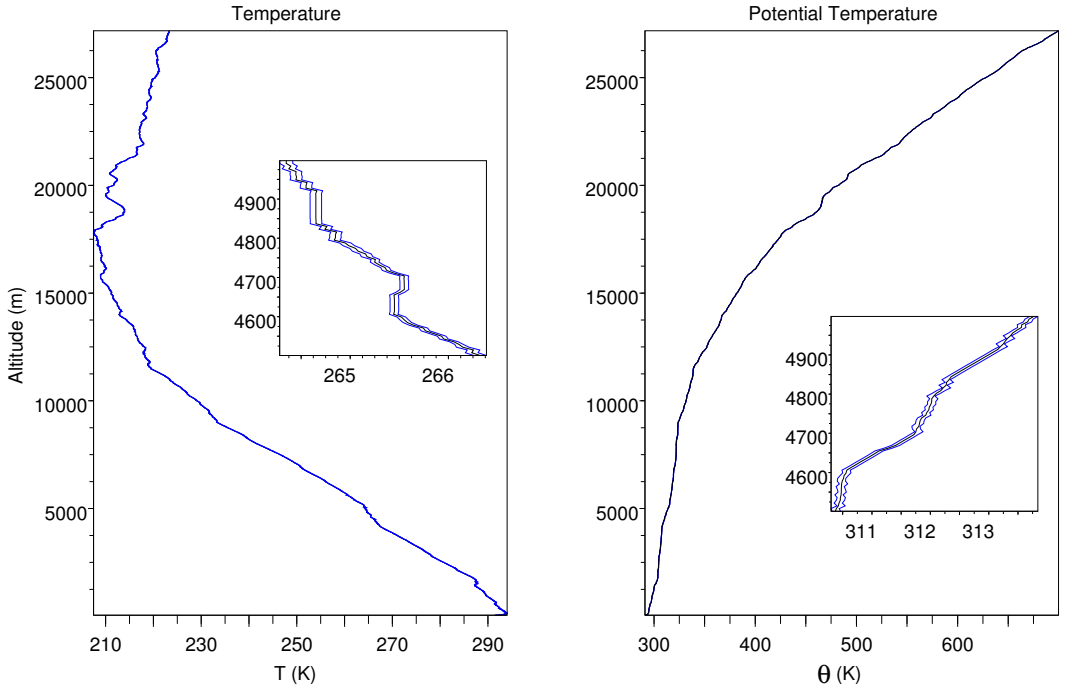

Fig. 2. Temperature profile (MUTSI-LR10 flight) (left). A magnification for the 4500–5000 m altitude domain is shown. Potential temperature profile (right).

AMTD
4, 969–1000, 2011

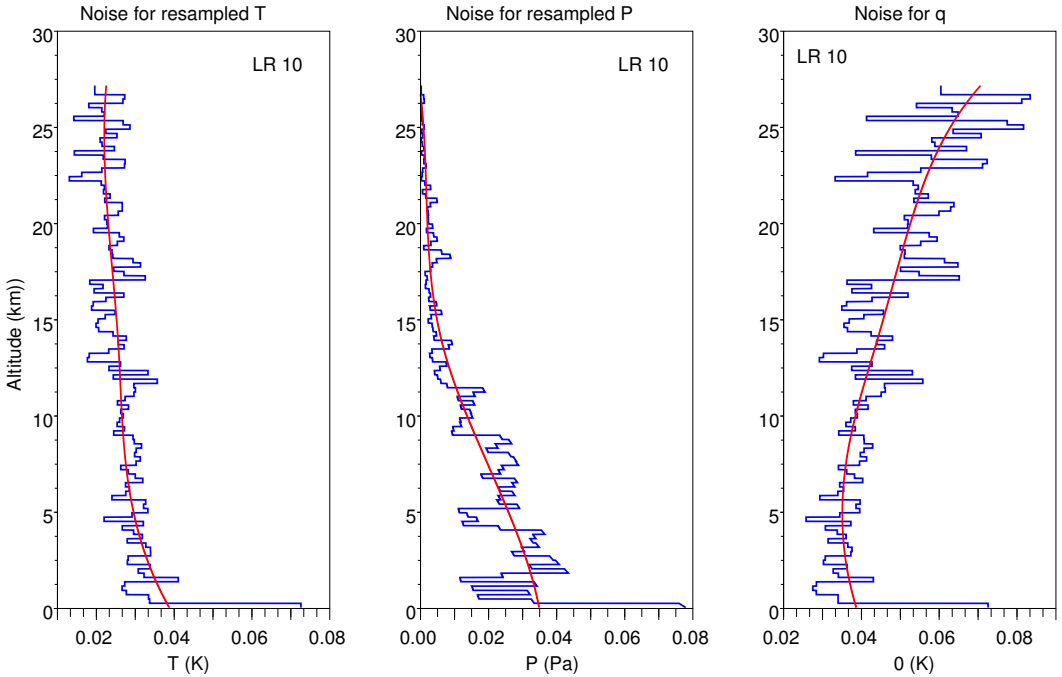

Fig. 3. Vertical profiles of the estimated level of noise for the MUTSI-LR10 flight of the temperature (left), the pressure (middle), the potential temperature (right). The noise level on potential temperature is inferred from the estimated noise on temperature and pressure. The blue curves show the estimates from data segments, the red curves showing smoothed profiles of these noise estimates obtained by spline approximations (see text).

AMTD
4, 969–1000, 2011

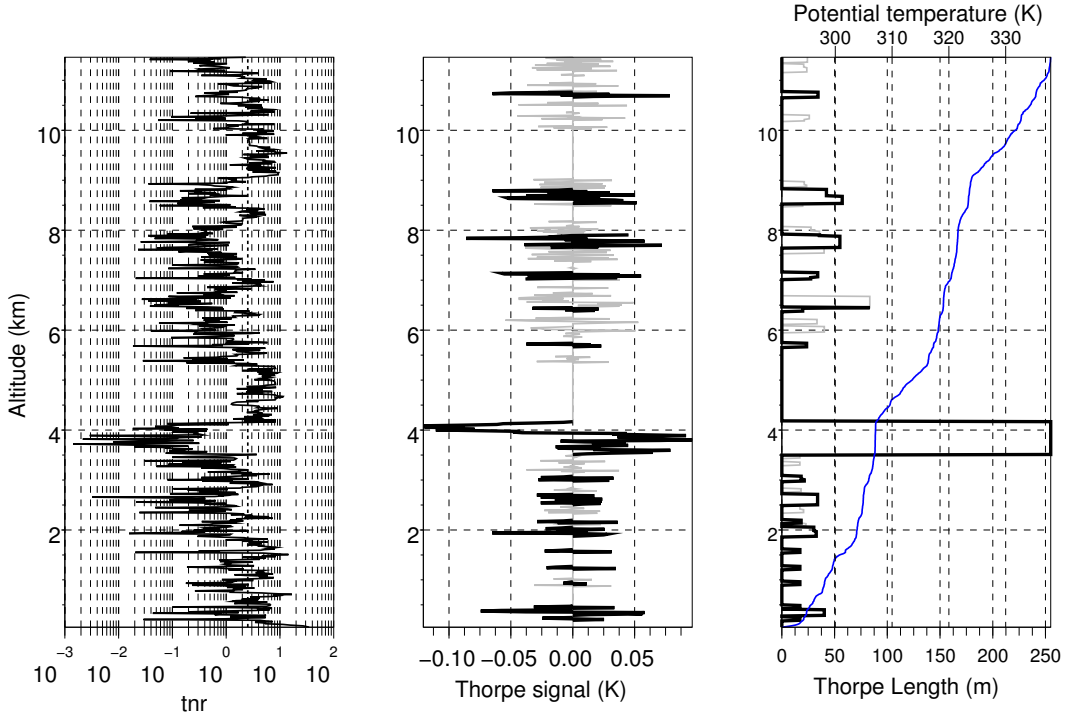

Fig. 4. MUTSI-LR10 flight: trend-to-noise ratio (left); Thorpe signal (middle); Thorpe lengths for the detected inversions (right). The selected overturns are highlighted.

AMTD
4, 969–1000, 2011

Small-scale turbulence from standard radiosondes

R. Wilson et al.

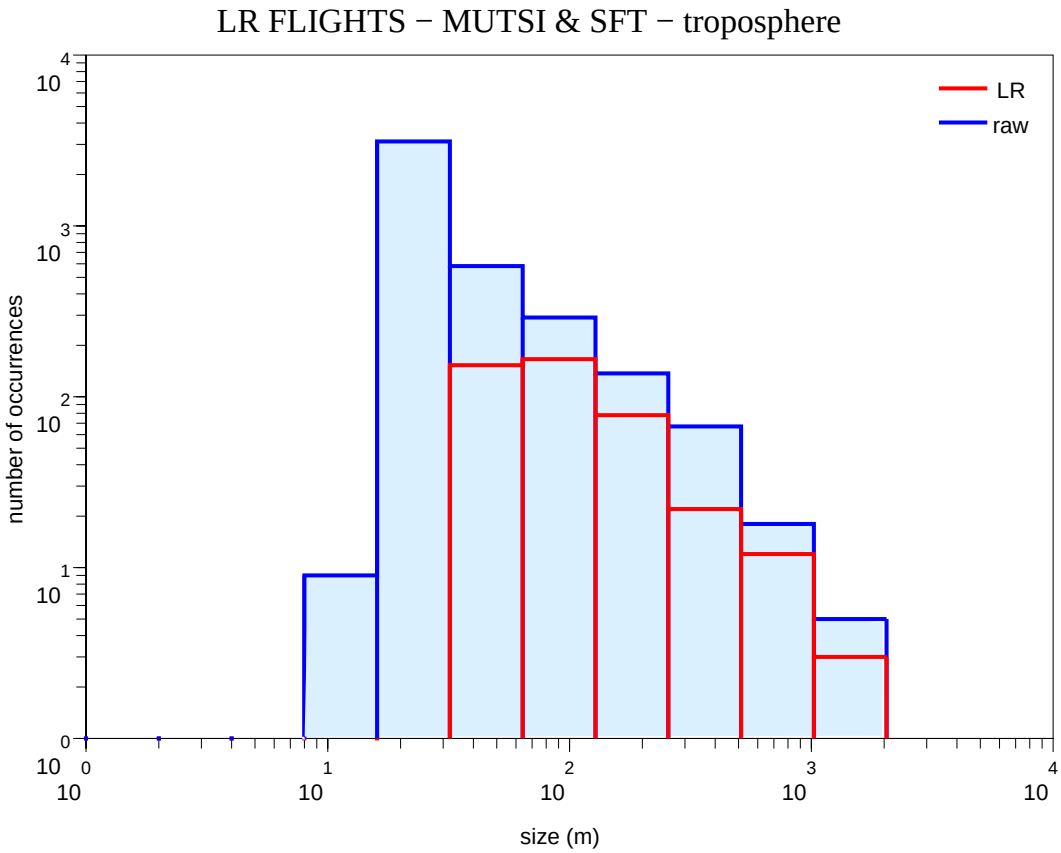

Fig. 5. Number of occurrences of the size of the detected inversions for all the LR profiles (blue-filled). Number of occurrences of the size of the selected overturns after applying a denoising and a selection procedure (red).

AMTD
4, 969–1000, 2011

Small-scale turbulence from standard radiosondes

R. Wilson et al.

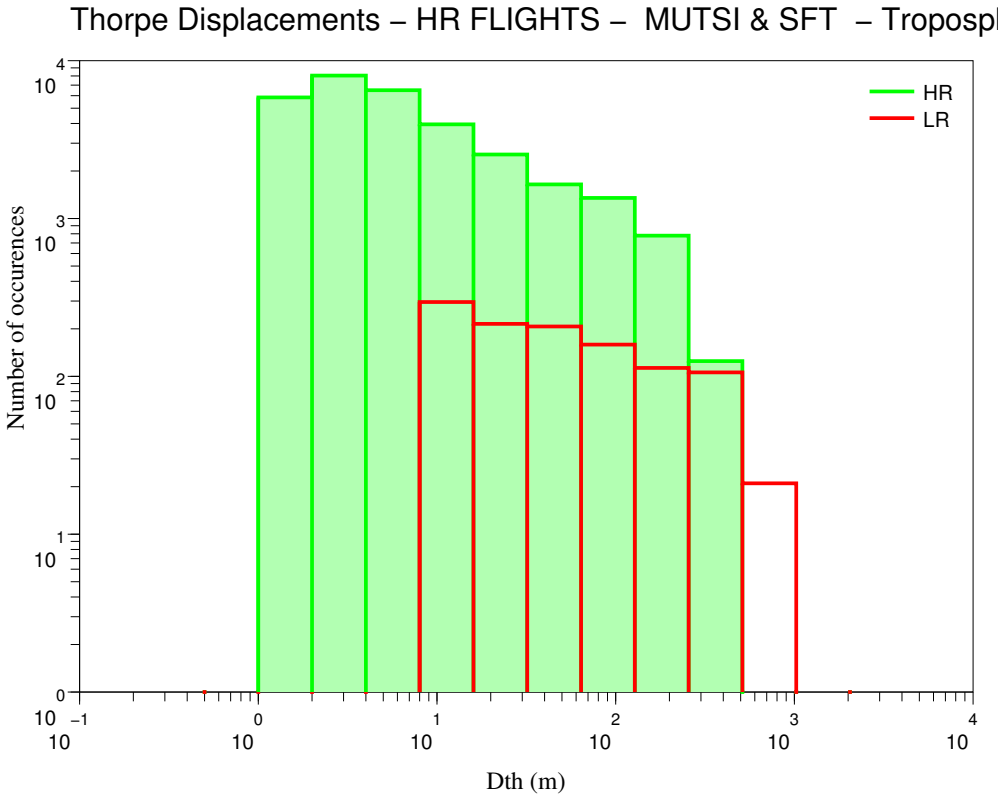

Fig. 6. Empirical distribution of Thorpe displacements within the selected overturns in the troposphere for the six HR flights of the MUTSI and SFT campaigns. The two histograms shows the distributions obtained from HR profiles (green-filled) and LR profiles (red-transparent).

AMTD
4, 969–1000, 2011

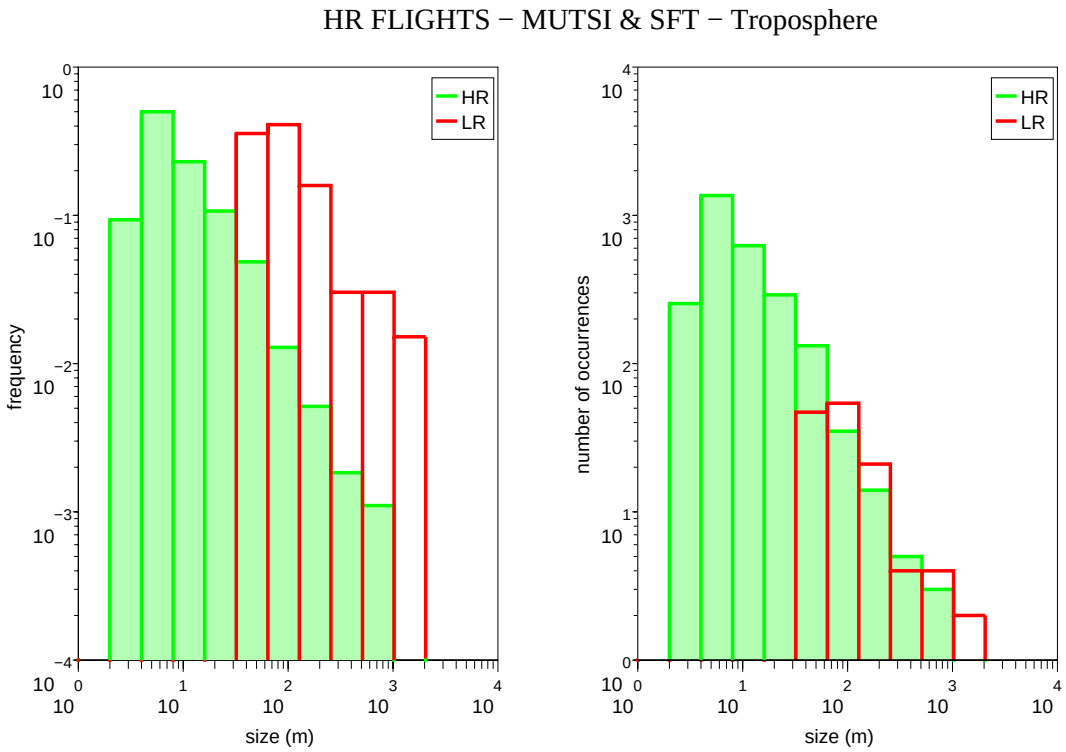

Fig. 7. Empirical probability of the size of overturns for the six HR flights of the MUTSI and SFT campaigns (left). Number of occurrences of the size of overturns for the same six flights (right).

AMTD
4, 969–1000, 2011

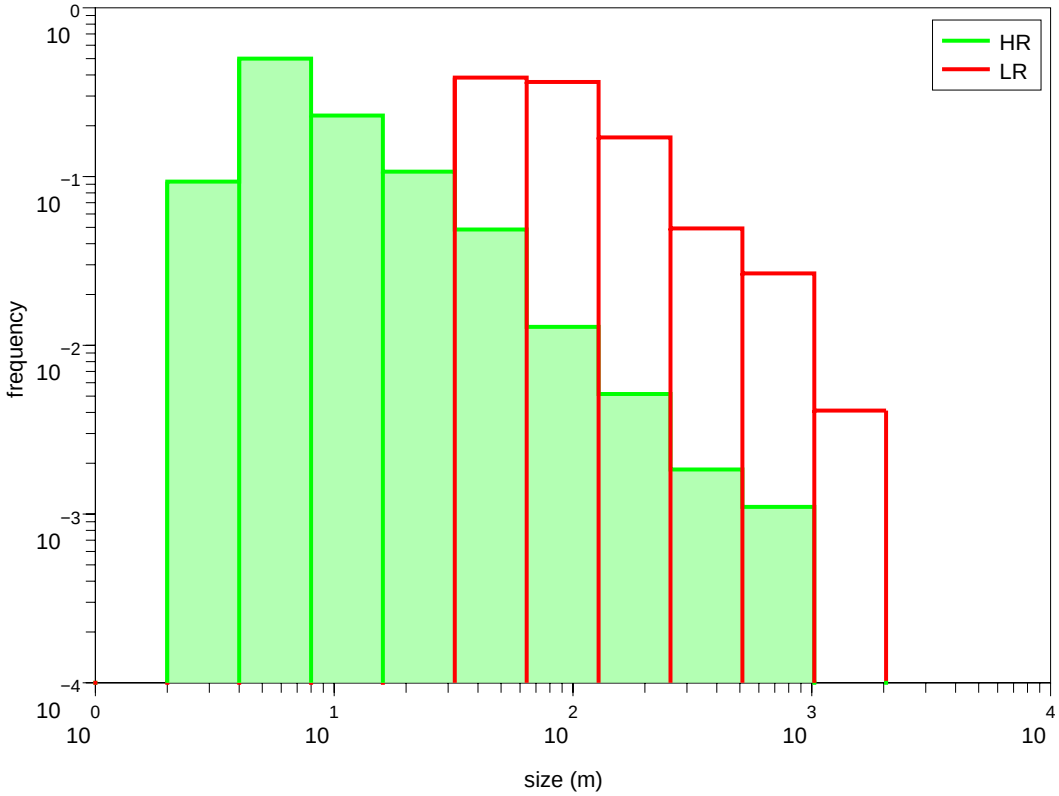

Fig. 8. Empirical probability of of the size of the overturns for all the flights of the MUTSI and SFT campaigns (6 HR and 20 LR flights).

AMTD
4, 969–1000, 2011

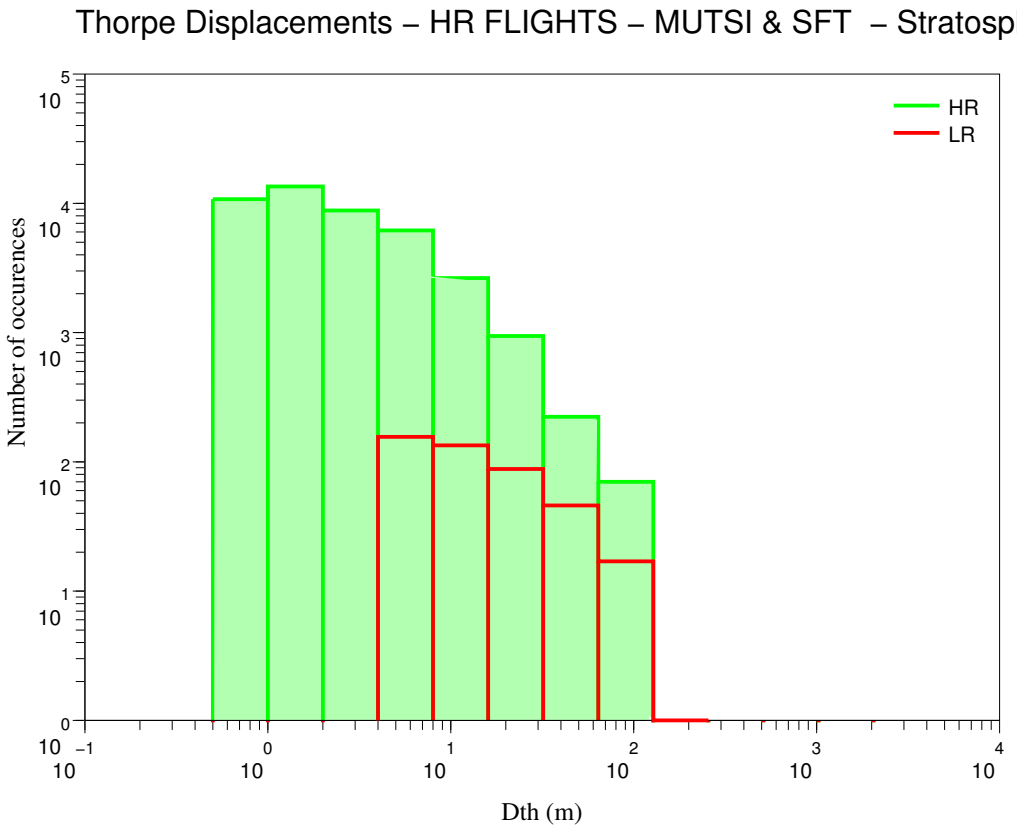

Fig. 9. Same as Fig. 6, but for the stratosphere.

AMTD
4, 969–1000, 2011

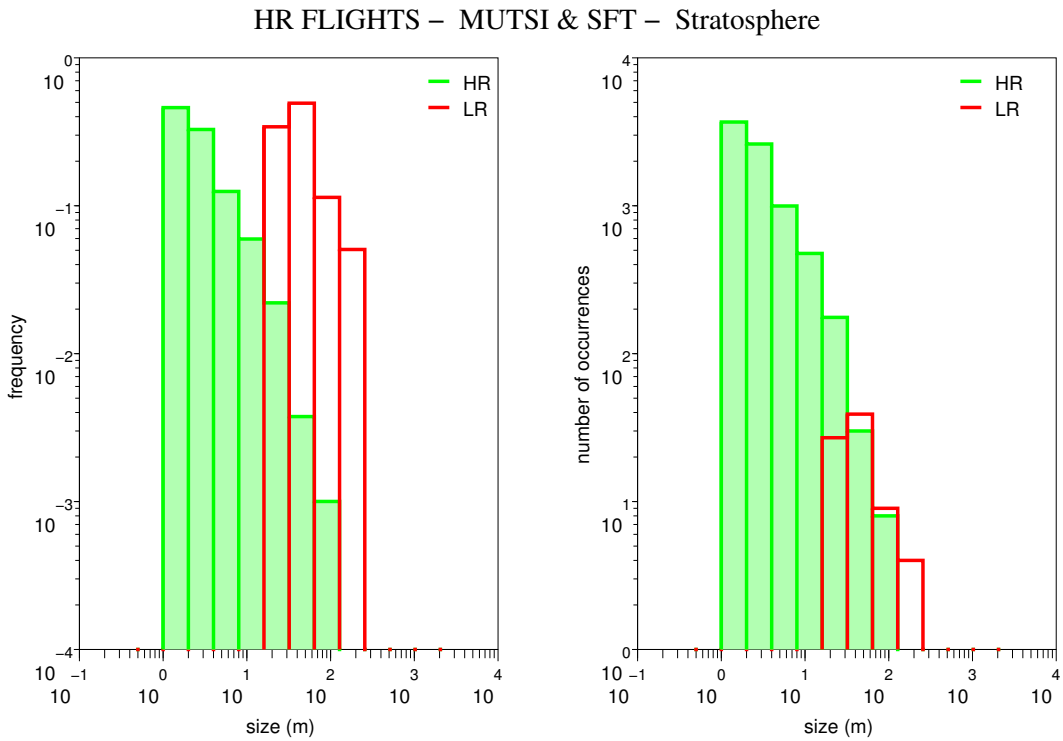

Fig. 10. Same as Fig. 7, but for the stratosphere.

AMTD
4, 969–1000, 2011

Small-scale turbulence from standard radiosondes

R. Wilson et al.

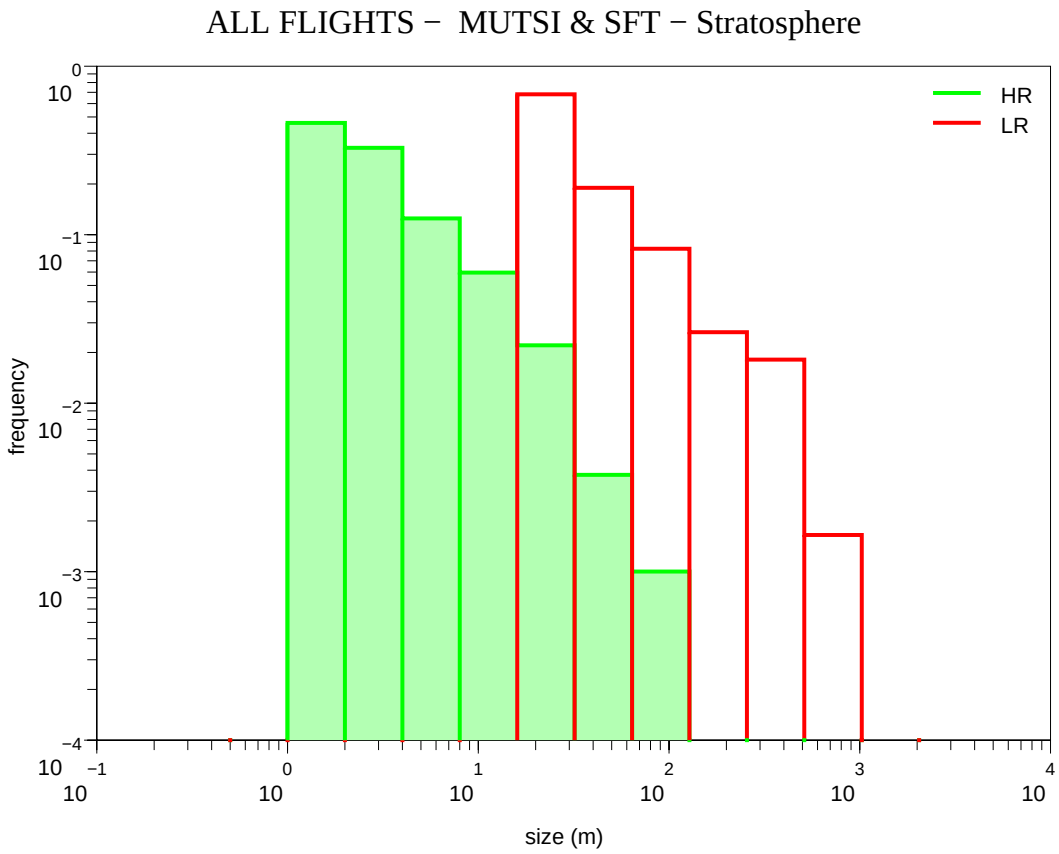

Fig. 11. Same as Fig. 8, but for the stratosphere.

AMTD
4, 969–1000, 2011

Small-scale turbulence from standard radiosondes

R. Wilson et al.